

# A Framework for Multi-source Privacy Preserving Epidemic Analysis

Zihan Guan<sup>1</sup>, Zhiyuan Zhao<sup>2</sup>, Fengwei Tian<sup>3</sup>, Dung Nguyen<sup>1</sup>,  
Payel Bhattacharjee<sup>3</sup>, Ravi Tandon<sup>3</sup>, B. Aditya Prakash<sup>2</sup>, Anil Vullikanti<sup>1</sup>

University of Virginia, Charlottesville, VA<sup>1</sup>  
Georgia Institute of Technology, Atlanta, GA<sup>2</sup>  
University of Arizona, Tucson, AZ<sup>3</sup>

## Abstract

It is now well understood that diverse datasets provide a lot of value in key epidemiology and public health analyses, such as forecasting and nowcasting, development of epidemic models, evaluation and design of interventions and resource allocation. Some of these datasets are often sensitive, and need adequate privacy protections. There are many models of privacy, but Differential Privacy (DP) has become a *de facto* standard because of its strong guarantees, without making models about adversaries. In this paper, we develop a framework that integrates deep learning and epidemic models to simultaneously perform epidemic forecasting and learning a mechanistic model of epidemic spread, while incorporating multiple datasets for these analyses, including some with DP guarantees. We demonstrate our framework using a realistic but synthetic financial dataset with DP; such a dataset has not been used in such epidemic analyses. We show that this dataset provides significant value in forecasting and learning an epidemic model, even when used with DP guarantees.

## 1 Introduction

Some of the common types of analyses done by epidemiologists and public health analysts include spatio-temporal analyses of diverse public health datasets, forecasting and nowcasting, development of epidemic models, evaluation and design of interventions, and resource allocation. These have become quite standard, especially after the pandemic, and libraries and cyberinfrastructures to facilitate such analyses have become commonplace. Diverse datasets are used in such libraries, and access has always been one of the most significant challenges in public health, but this changed during the pandemic. Many such datasets, e.g., on surveillance, mobility, and behaviors, provided significant public health benefits. However, many of these datasets are quite sensitive, but became available and got shared quite easily, without due privacy considerations. There has been a significant recognition of the importance of ensuring the privacy of datasets used in such analyses, as emphasized in the 2023 US President’s Executive Order [46] and the EU General Data Protection Regulation (GDPR) [14].

Providing privacy protections, is however, very challenging. There are many models of privacy, and here we focus on differential privacy (DP), which has emerged as the *de facto* standard notion for privacy, and is used by US Census and industry [7, 15, 16, 36] (and has also been highlighted in the 2023 [46]). Despite a lot of work on privacy-enhancing techniques (including DP), their use in epidemiology and public health has been quite limited. This limitation has been recognized through recent challenges on public health analyses with DP: the US-UK PET challenge for public health, run by NSF and NIST [37, 21] and the “PETs for Public Health Challenge” [1].

Our novel contribution is a powerful framework, DPEPINN, for supporting a broad class of epidemic analyses using diverse types of datasets, with DP guarantees. A key aspect of DPEPINN is an integration of deep learning with an epidemic model, and simultaneously performs forecasting of epidemic metrics and

Dataset	Metrics ↓	Baseline Method	Public Setting		Private Setting	
		LSTM	w/o Transaction	w/ Transaction	RR	Laplacian
Bogotá	RMSE	302.14	350.63	285.69	323.76	233.94
	MAE	251.86	319.35	302.25	255.59	289.66
Medellín	RMSE	237.65	216.40	186.74	225.25	256.27
	MAE	223.22	174.89	150.68	180.51	211.72

Table 1: Overall forecasting performance comparison of all the settings, without and with privacy with  $\epsilon = 1$  for the RR and Laplacian mechanisms.

learns a good epidemic model. Further, this framework allows the integration of very heterogeneous types of datasets, including those which have privacy requirements. Here we use a realistic but synthetic financial dataset released by data.org<sup>1</sup> as part of a “PETs for public health challenge” [1]; we refer to this dataset as the “transaction dataset” in rest of the paper. The transaction dataset provides merchant-level credit card transaction data for a few South American cities during the COVID period; This data is used here with DP guarantees.

Typically, datasets used in constructing epidemic models are used to infer different components, such as epidemic state (e.g., from surveillance-type data), or mixing rates (from mobility-type datasets). The use of transaction data is a challenge since it is not easy to map it to components of the epidemic model. A strength of our framework is its ability to incorporate this dataset, along with other diverse datasets.

### Summary of main results.

- We find that the transaction dataset does have useful predictive power for forecasting and learning epidemic models (even after the transformations done by data.org), as our results for Bogota and Medellin, Colombia show (Table 1).

For Bogota, this holds even when the financial dataset is used with DP; our two private methods have significantly better performance than not using the financial dataset. For Medellin, the DP solutions have slightly higher errors. This is consistent with other efforts using DP, and privacy-utility tradeoffs can vary significantly depending on the datasets and problems.

- A strength of our framework is that very diverse datasets can be directly incorporated for both forecasting and learning epidemic models. In addition to epidemic datasets (cases and mortality), we use Google Health Trends, Google Mobility, and transaction data. We find that the Google mobility data gives an improvement in the RMSE in some cases, though this is not very consistent (Table 5).
- We demonstrate the utility of the privately learned epidemic model through a case motivated by public health questions. We perform a counterfactual analysis of a social distancing type intervention which leads to a reduction in transmission rate by a given amount, starting at a fixed time (Section 4.4). Our analysis (Figure 5) shows a higher sensitivity to the level of social distancing adaptations. While there is no ground truth for such analysis, our results have greater support because we achieve a better model fit using the financial dataset with DP. Such an analysis can give insights to public health analysts about how the epidemic is spreading, and the potential impact of policies.

**Data availability.** All the public datasets we use are listed and are fully available. The transaction dataset, which was used in this work, is private and is not available.

## 2 Background

We briefly describe the background and notation needed for the remaining discussion here.

<sup>1</sup>The data provided for this research is supplied as-is, with no warranties or guarantees, and the data provider holds no liability for its accuracy, completeness, or any consequences arising from its use.

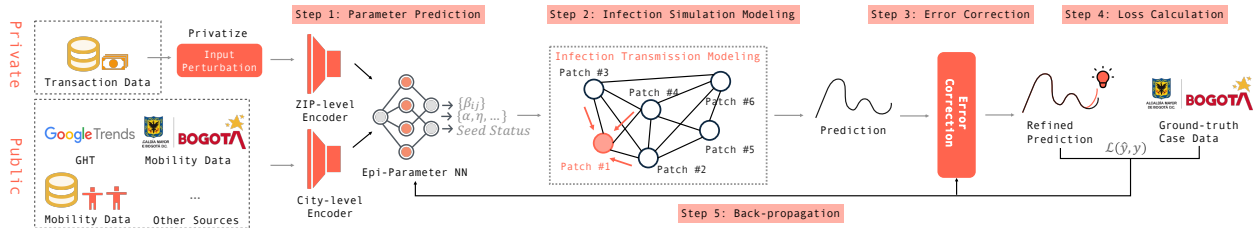


Figure 1: DPEPINN: This consists of three modules: PARAMETERNN, Meta-population Model, and Error Correction Adapter. Datasets are processed by the PARAMETERNN modules to generate epidemic parameters using multiple encoders. The first encoder processes the city-level dataset, incorporating public features such as city-level cases, deaths, and Google health trends. The second encoder handles the zipcode-level dataset, utilizing privatized features from the transaction dataset. The embeddings from both encoders are concatenated and passed to the decoder. These parameters are then input into the meta-population model to generate pandemic simulations. An error correction adapter further corrects errors in the simulations adaptively.

Many of the datasets we use (and others commonly used in epidemiology) are spatial, and here we focus on zipcodes (also referred to as postal codes in some of the South American cities that we consider here). Let  $Z$  denote the set of zipcodes. For a given time stamp  $t$  (which would be at the level of days), let  $y_{i,t}$ ,  $m_{i,t}$ ,  $x_{i,t}^{pub}$  and  $x_{i,t}^{priv}$  denote the number of infections, number of deaths, tensor of public features, and a private dataset, respectively, for  $i \in Z$ ; we use  $\mathbf{y}_t$ ,  $\mathbf{m}_t$ ,  $\mathbf{x}_t^{pub}$  and  $\mathbf{x}_t^{priv}$  to denote the corresponding tensors (over all groups). Let  $\mathbf{y}_t = \sum_{i \in Z} y_{i,t}$  and  $\mathbf{m}_t = \sum_{i \in Z} m_{i,t}$  denote the total number of infections and deaths, respectively, at the city level. We summarize the main epidemiological analyses we consider.

**Forecasting.** The goal in the forecasting problem is to use data till time  $T$ , namely  $\{\mathbf{y}_t\}_{t=1}^T$ ,  $\{\mathbf{m}_t\}_{t=1}^T$ ,  $\{\mathbf{x}_t^{pub}\}_{t=1}^T$  and  $\{\mathbf{x}_t^{priv}\}_{t=1}^T$ , and predict  $\{\mathbf{y}_t\}_{t=T+1}^{T+H}$  and  $\{\mathbf{m}_t\}_{t=T+1}^{T+H}$  i.e., the number of infections and deaths during the time period  $[T+1, T+H]$ , where  $H$  is the forecast horizon. Here, we only consider city-level predictions.

**Epidemic models.** We consider different kinds of epidemic models, denoted by  $M_{inf}(\mathbf{p})$  (with  $\mathbf{p}$  denoting the vector of parameters), including agent-based models, e.g., [29, 22], and metapopulation models, e.g., [34, 47]. A structured metapopulation model represents the transmission of a disease within a set  $\mathcal{G}$  of groups; depending on the questions of interest and data, different kinds of groups can be considered, e.g., based on age groups or population in a zip code. We describe the simplest such SEIRM metapopulation model,  $M_{inf}(\mathbf{p})$ , for the evolution of infections  $\mathbf{y}_t$  and deaths  $\mathbf{m}_t$  in Section 3.1.2, along with how it is used in our approach. This can be easily extended to include other states and interventions; we refer to [29, 22] for discussion on ABMs.

**Privacy models.** Let  $\mathcal{D}^{priv}$  denote a set of datasets whose privacy needs to be protected;  $\mathcal{D}$  consists of the private temporal datasets  $\mathbf{x}_t^{priv}$ . We aggregate private datasets at the level of zipcodes, so for the financial dataset,  $x_{i,t}^{priv}$  is the sum of all transactions (for a particular category) in zipcode  $i$ .

We say that a (randomized) algorithm  $M : \mathcal{D} \rightarrow \mathcal{R}$  satisfies  $(\epsilon, \delta)$ -DP if for all subsets  $S \subset \mathcal{R}$ , and for all  $D, D' \in \mathcal{D}$  with  $D \sim D'$ , we have  $Pr[M(D) \in S] \leq e^\epsilon Pr[M(D') \in S] + \delta$  [16]. Simply put, a DP mechanism ensures that the result changes in a controlled manner if the dataset is changed from  $D$  to its neighbor  $D'$ . For private temporal datasets, we consider focusing on the stronger user-level privacy model: here  $D, D'$  differ in the data associated with a single user (this was a requirement in the PET challenge [1]). For the financial dataset, this corresponds to a single merchant. Another simpler, privacy model is event-level privacy, where  $D, D'$  differ in the data associated with a single event.

### 3 Our approach

Our DPEPiNN pipeline is illustrated in Figure 1 and consists of three modules described in § 3.1: (1) a PARAMETERNN that calibrates the epidemic parameters for the Metapopulation model; (2) a Metapopulation model for epidemic simulation and prediction; and (3) an error correction adapter that further refines the prediction. Additionally, the private transaction dataset is processed by an input perturbation module described in § 3.2.

#### 3.1 DPEpiNN for learning epidemic models and forecasting dynamics

##### 3.1.1 Differentiable meta-population model overview

Real-world epidemiological forecasting problems typically require both forecasting accuracy and interpretability [30]. However, existing methods often rely exclusively on either mechanistic models, such as meta-population or agent-based models, or deep neural networks, such as recurrent networks and transformers, making it difficult to achieve both goals within a single model. On the one hand, while mechanistic models offer strong interpretability, they suffer from limited forecasting accuracy due to their inherent model capacity constraints. On the other hand, although deep neural models can provide accurate predictions, their black-box nature offers little interpretability, which is crucial for epidemiologists and decision-makers.

Several approaches have been proposed that integrate agent-based models with neural networks for parameter calibration [12, 5]. However, these methods often face scalability challenges and are typically limited to micro-level scenarios, such as simulating infections within a hospital. In contrast, epidemiological forecasting also demands models capable of operating at a macro level while maintaining both accuracy and interpretability. To this end, we propose DPEPiNN, a differentiable meta-population framework that addresses both concerns while ensuring practical applicability in macro-level disease forecasting.

The proposed DPEPiNN framework consists of three key components: First, a **parameterNN**, which takes both public and private data from diverse sources as input and outputs time-varying parameters for the mechanistic model. By leveraging multiple data sources rather than relying solely on the target time series, ParameterNN enables more accurate parameter calibration and better trend extraction. Second, a **meta-population model** that captures interactions between different groups, such as age groups or geographic regions. Unlike agent-based models, which operate at a finer scale, the meta-population model offers flexibility in selecting groups at different levels of granularity, enhancing its adaptability for broader forecasting applications. Third, a **forecasting adaptor** is designed to correct forecasting predictions adaptively. While the meta-population model, combined with ParameterNN, can lead to over-calibration due to the data richness—resulting in degraded forecasting accuracy—the adaptor mitigates such overfitting issues, improving overall predictive performance.

##### 3.1.2 Epidemic Model

Here, we describe the modeling of the meta-population model. A meta-population model is a multi-patch extension of the simple SEIRM model, allowing a more fine-grained simulation of interactions between a set  $\mathcal{G}$  of groups, such as the pandemic transmission, in the given region. An example is groups correspond to the population in specific age groups; age-stratified data is publicly available<sup>2</sup> and has been shown to be a reliable signal for epidemic forecasting [20].

A meta-population model requires two key inputs: a contact matrix  $\mathcal{C} \in \mathbb{R}^{m \times m}$  and a population vector  $N \in \mathbb{R}^m$ , where  $m = |\mathcal{G}|$  is the number of groups. Each entry  $C_{i,j} \in \mathcal{C}$  represents the contact probability between the populations in groups  $i$  and  $j$ , while each entry  $N^j \in N$  records the population of group  $j$ . Following [47], the effective number of infected individuals and the effective population of group  $j$  after daily movement are defined as:

$$I_j^{\text{EFF}} = \sum_i C_{i,j} I_i, \quad N_j^{\text{EFF}} = \sum_i C_{i,j} N_i \quad (1)$$

---

<sup>2</sup><https://github.com/NSSAC/PatchSim/tree/master>

where "EFF" (effective) refers to infections accounted including infected individuals between different sub-populations due to transmissibility and mobility. The conditional force of infection for group  $j$  is then given by:

$$\beta_j^{\text{EFF}} = \beta \frac{I_j^{\text{EFF}}}{N_j^{\text{EFF}}}. \quad (2)$$

For each group  $i \in [1, \dots, m]$ , the epidemic evolution  $\mathcal{Z}_i = [S_i, E_i, I_i, R_i, M_i]$  from day  $t$  to day  $t + 1$  is formulated as:

$$\begin{aligned} \mathcal{Z}_i(t+1) &= \mathcal{Z}_i(t) + \Delta \mathcal{Z}_i(t), \quad \text{where} \\ \Delta S_i(t) &= - \sum_{j=1}^m C_{i,j} \beta_j^{\text{EFF}} S_i(t) + \delta(t) R_i(t), \\ \Delta E_i(t) &= \sum_{j=1}^m C_{i,j} \beta_j^{\text{EFF}} S_i(t) - \alpha(t) E_i, \\ \Delta I_i(t) &= \alpha(t) E_i(t) - (\gamma(t) + \eta(t)) I_i(t), \\ \Delta R_i(t) &= \gamma(t) I_i(t) + (1 - \delta(t)) R_i(t), \\ \Delta M_i(t) &= \eta(t) I_i(t). \end{aligned} \quad (3)$$

where our forecasting objective  $\Delta I_i(t)$  represents the number of newly infected individuals in age group  $i$  at time  $t$ . Running the meta-population model for  $T$  time steps, it outputs the aggregated new cases over all the age groups for the entire training period:

$$\hat{y}_t := \sum_{i=1}^m \Delta I_i(t), \forall 1 \leq t \leq T. \quad (4)$$

### 3.1.3 parameterNN

The meta-population model incorporates a large number of time-varying hyperparameters, such as  $\alpha(t)$ ,  $\gamma(t)$ , and  $\eta(t)$  for the pandemic transmission simulation. Despite the challenge brought by these complex parameters, accurate calibration time-dependently becomes even more challenging, especially when the total time step  $T$  is large. Consequently, the vast search space makes calibrating these epidemic parameters highly challenging, often requiring manual efforts or relying on traditional calibration strategies such as EAKF [8], which frequently fail. Motivated by the recent success of differentiable calibration methods [12], we propose a DNN-based approach that predicts epidemic parameters from given datasets. Intuitively, our goal is to train a neural network model,  $f_{\theta_{\text{epi}}}$ , capable of capturing pandemic trends through these predicted epidemic parameters.

In our setup, we incorporate both the public datasets, such as city-level Google Health Trends, Google Mobility Dataset, and Infection Statistics, and the private ones are more fine-grained zip-level datasets from credit transaction data. To simultaneously handle both granularity and generate time-varying epidemic parameters, our neural network  $f_{\theta_{\text{epi}}}$  is designed to be a two-encoder-based sequence model so that it can encode the zip-level information and the City-level information separately. Let  $\mathcal{D}_{\text{tran}}$  denote the private transaction dataset, and  $\mathcal{D}_{\text{public}}$  denote the merged public dataset, we get the predicted epidemic parameters  $p(t) := \{\alpha(t), \gamma(t), \eta(t), \dots\}$  as follows:

$$\{p(t)\}_{t=1}^T = f_{\theta_{\text{epi}}}(\mathcal{D}_{\text{tran}}, \mathcal{D}_{\text{public}}). \quad (5)$$

To improve the learning stability in the training process, we only update  $p(t)$  on a weekly basis, i.e.,  $p(t) = p(t')$  for  $t, t' \in \{7i+1, \dots, 7(i+1)\}$ , for all  $i$ , though the forecasts and epidemic model runs at a daily level. More details on the model architecture are provided in the Appendix.

### 3.1.4 Error Correction Adapter

While the proposed PARAMETERNN enhances interpretability for historical calibration, it tends to suffer from reduced forecasting accuracy due to the lack of calibration in the horizon time series. To address this issue, we design a novel correction adapter module that locally aligns the simulation with the ground-truth epidemic curves to refine the simulation in the horizon window. Formally, given a simulation sequence  $\hat{y}$  of length  $T$ , the error correction adapter first partitions the sequence into overlapping contiguous chunks of size  $k$ . Each chunk, defined as  $\text{chunk}_j = \{\hat{y}_j, \hat{y}_{j+1}, \dots, \hat{y}_{j+k-1}\}$ , captures a short time window of the simulation for localized correction. This approach allows the adapter to focus on refining small segments of the sequence rather than attempting a global adjustment all at once. Next, the adapter predicts a corrected value for each chunk based on its historical simulation data, using a network  $g_\theta$  parametrized by  $\theta$ , i.e.,  $\tilde{y}_j = g_\theta(\text{chunk}_j)$ . By applying this correction iteratively across all chunks, we obtain a refined sequence of adjusted values,  $\{\tilde{y}_j\}_{j=1}^{T-k}$ , which better reflects the expected epidemic trajectory.

### 3.1.5 Loss Calculation

Given the simulation  $\{\hat{y}_t\}_{t=1}^T$  and the refined simulation  $\{\tilde{y}_t\}_{t=1}^{T-k}$ , we can calculate two loss functions:

$$\mathcal{L}_{MetaPop} = \frac{1}{T} \sum_{t=1}^T \|\hat{y}_t - y_t\|_2, \quad (6)$$

and

$$\mathcal{L}_{Adapter} = \frac{1}{T-k} \sum_{t=1}^{T-k} \|\tilde{y}_t - y_{t+k}\|_2, \quad (7)$$

respectively. Combining the two losses together with a linear rate  $\alpha$ , we get

$$\mathcal{L} = \alpha \cdot \mathcal{L}_{MetaPop} + (1 - \alpha) \cdot \mathcal{L}_{Adapter}. \quad (8)$$

To train the whole pipeline, one can simply back-propagate with the gradients of loss value defined in Equation 8.

However, it is generally challenging to select an optimal  $\alpha$  value. Moreover, using a constant  $\alpha$  is more likely to result in convergence issues. Therefore, instead of maintaining a constant  $\alpha$  throughout all training epochs, we propose defining  $\alpha_t$  as a function of the training epoch  $t$ . Specifically,

$$\alpha_t = \frac{t}{T}, \quad (9)$$

where  $T$  denotes the total training epochs. Intuitively,  $\alpha_t$  is a linearly increasing function of the training epoch  $t$ . During the early stages of training, the weight assigned to the PARAMETERNN module is relatively larger. Gradually, this weight shifts toward the adapter module. This design is based on our empirical observation that the PARAMETERNN module converges more slowly than the adapter module. Assigning a larger weight to this module during the early training stages promotes more stable loss reduction.

**Remark 1 (Implementation Optimization)** *We empirically find that, the prediction performance of the DPEPINN can be enhanced by using a three-stage training strategy. Specifically, in the first stage, we only train the PARAMETERNN with the loss in Equation 6, which will secure an accurately calibrated simulation. Then in the second stage, we only train the error correction adapter with the loss in Equation 7, which encourages the model to focus on improving its correction capability. Finally, the model is trained on a combination loss defined in Equation 8 with a few more epochs, which provides further space for simultaneously adjusting the two simulations.*

## 3.2 Privacy mechanisms

Due to the mixed nature of our public and private datasets, we employ two input perturbation techniques to ensure privacy. Our private transaction data, including zip codes and transaction amounts, are both considered sensitive and require privacy protection. This means the location (zip code) and the amount of each individual transaction must be kept private. Furthermore, because each merchant may have transactions at multiple locations, a composition mechanism is necessary to provide merchant-level privacy. As shown in Figures 2 and 1, input perturbation is applied to the transaction data, which is then used for training.

### 3.2.1 Privacy via the Laplace mechanism

We use transaction data aggregated by amount (for specific categories) at the level of zip codes and weeks. This aggregated dataset, denoted by table  $D^{Tran}$ , consists of  $M$  rows, where row  $i$  represents a postal code  $P_i$  (for a total of  $M$  postal codes:  $P_1, \dots, P_M$ ).  $D^{Tran}$  has 209 columns, each representing a specific week in our time series of historical transaction data. The value in cell  $D_{ij}^{Tran}$  represents the total amounts of transactions in postal code  $P_i$  during week  $j$ . We clip each original transaction amount by a pre-determined maximum amount of  $C$ , such that any transaction amount that is greater than  $C$  will be treated as  $C$ .

To calculate the sensitivity of table  $D^{Tran}$ , note that removing one merchant from the mock data can remove up to  $K = 627$  records in the worst case, which makes the global  $\ell_1$ -sensitivity of  $D^{Tran}$  to be  $627 \times C$ . Therefore, adding a Laplacian noise with magnitude  $\frac{627 \times C}{\epsilon}$  to each cell of  $D^{Tran}$  satisfies  $\epsilon$ -DP.

### 3.2.2 Privacy via label DP using Randomized Response

We consider another approach for input perturbation based on Label DP [17], which aims to provide a differential privacy guarantee only for the specific label. Informally, the goal of label DP is to ensure the influence of any individual data entry’s label on the trained model is limited, in this case, the specific pair of merchant ID and postal code. This limits the ability of an adversary to infer the true label of any given data point, thereby protecting sensitive information while maintaining the utility of the overall model. Formally, the notion of Label DP is defined as:

**Definition 1** ( $\{\epsilon, \delta\}$  **Label Differential Privacy**) *For all two neighboring datasets  $\mathcal{D}, \mathcal{D}'$  that differs in the label of a single data entry, and for any subset  $\mathcal{S}$  of outputs of randomized algorithm  $\mathcal{M}$ , the algorithm  $\mathcal{M}$  is  $(\epsilon, \delta)$ -Label Differentially Private (Label DP) for  $\epsilon \geq 0$  and  $\delta \in [0, 1]$  if:*

$$\mathbb{P}[\mathcal{M}(\mathcal{D}) \in \mathcal{S}] \leq e^\epsilon \cdot \mathbb{P}[\mathcal{M}(\mathcal{D}') \in \mathcal{S}] + \delta.$$

The idea here is to privatize the zip codes and the transaction data separately to provide event-level privacy and use composition to provide merchant-level privacy. First, we implement randomized responses on the zip codes with a privacy budget of  $\epsilon_{zip}$ . Next, to preserve the privacy of the transaction data (transaction details), we used both quantization and randomized response. Based on the bin size  $B$ , we divided the entire transaction data into  $B$  bins and implemented a randomized response with a privacy budget of  $\epsilon_{trans}$ . This proposed methodology provides  $\epsilon_{event}$  event-level privacy with basic composition as:

$$\epsilon_{event} = \epsilon_{zip} + \epsilon_{trans} \tag{10}$$

**Randomized response with quantization.** We essentially propose two different privacy budgets for zip code and transaction details. This process involves reporting the zip code with a probability of  $\frac{e^{\epsilon_{zip}}}{e^{\epsilon_{zip} + k_1} - 1}$  and reporting another random zip code uniformly with a probability of  $\frac{1}{e^{\epsilon_{zip} + k_1} - 1}$ . Here,  $k_1$  represents the cardinality of the set of all possible zip codes. For transaction details, we first quantize the data into  $B$  bins and then apply randomized response with a privacy budget of  $\epsilon_{trans}$ . Without a doubt, the number of bins  $B$  will influence the utility of the data; by setting  $B = 1$  will preserve perfect privacy on transaction details. For practical reasons,  $B$  is pre-determined to be 50, although this parameter can be tuned for different performance requirements or datasets. Therefore, this mechanism returns the true quantized transaction data with probability  $\frac{e^{\epsilon_{trans}}}{e^{\epsilon_{trans} + B} - 1}$  and reports another random quantized transaction data uniformly with

Dataset	Period	Starting	Ending
Bogotá	Training	2020-03-01	2021-02-14
	Testing	2021-02-15	2021-03-14
Medellín	Training	2020-03-01	2021-02-14
	Testing	2021-02-15	2021-03-14

Table 2: Starting date and ending date of the training and testing period for the Bogotá and Medellín dataset.

probability of  $\frac{1}{e^{\epsilon_{\text{trans}}} + B - 1}$ . However, this method does not rely on prior knowledge of the dataset, specifically does not rely on the distribution of zip codes and transaction details.

**Merchant-level Privacy.** For this notion of privacy, we assume  $D \sim D'$  if they differ in entries corresponding to exactly one merchant. To achieve merchant-level privacy, we have to take into account the composition cost due to the multiple appearances of each unique merchant in the transaction dataset. Since there are 209 weeks and each merchant has at most 3 postal codes, a merchant may contain up to  $K = 209 \times 3 = 627$  transaction entries.

**Reduction in privacy cost using sub-sampling.** Sub-sampling offers an additional avenue for enhancing privacy. Basic composition dictates a merchant-level privacy budget of  $K\epsilon_{\text{event}}$ . However, by selecting only  $\alpha$  fraction of transactions for each zip code and date, the privacy budget is reduced to  $K\alpha\epsilon_{\text{event}}$  [18]. In order to achieve  $\epsilon = 1$ , we choose  $\epsilon_{\text{event}} = 0.007$  for  $\alpha = 0.2$  for practicality.

## 4 Results

### 4.1 Experimental Setups

#### 4.1.1 Heterogeneous Data Sources

In the experiments, we focus on epidemic forecasting for two locations: Bogotá and Medellín. For both of the two locations, we collected datasets from three sources: (1) Daily cases and deaths data provided by the National Institute of Health of Colombia<sup>3</sup>, (2) Search trends for symptoms from Google Health Trends<sup>4</sup>, with keywords such as "covid-19 en Colombia", "covid-19 vacuna", "covid-19 hoy", and "covid-19 Bogotá", and (3) Google Mobility Dataset<sup>5</sup> with 6 features relevant to mobility changes in different scenarios. Apart from these public datasets, we also consider the transaction dataset released by data.org [1]; each entry records the zip code, category, time, and spending amount of transactions for the given location. To utilize this transaction dataset, we preprocess it by aggregating the sum of the spending amounts across all categories, resulting in a dataset relevant only to zip code and time. We consider a default training period of 49 weeks, which starts from 2020-03-01. The following Table 2 summarizes the starting and ending date for training and ending period, respectively. The prediction horizon is set as 28 days. For the testing stage, we evaluate the model's performance by comparing infection predictions (i.e., 28 days following the training stage) with the ground-truth infection values.

#### 4.1.2 Metrics

For performance evaluation, we use three popular metrics, including root mean square error (RMSE), mean absolute error (MAE), and mean absolute percentage error (MAPE). For any given prediction  $\mathbf{y}'_t$  and the

<sup>3</sup><https://www.ins.gov.co/Noticias/Paginas/coronavirus-casos.aspx>

<sup>4</sup><https://trends.google.com/trends/explore?date=today>

<sup>5</sup>[https://www.gstatic.com/covid19/mobility/Global\\_Mobility\\_Report.csv](https://www.gstatic.com/covid19/mobility/Global_Mobility_Report.csv)

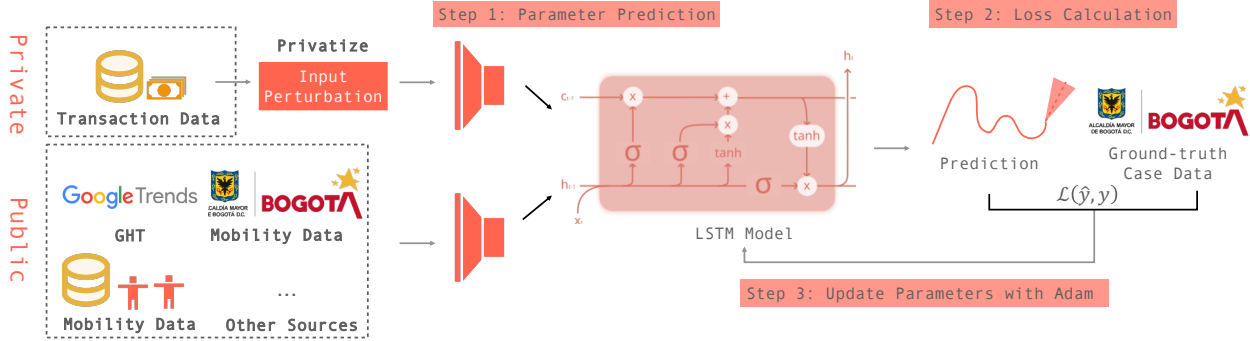


Figure 2: Forecasting using the LSTM technique: we use a multi-encoder structure, which allows different types of datasets (whose shapes are not always consistent) to be incorporated. Transaction data is incorporated through a separate encoder. Predictions are generated directly by the LSTM in an autoregressive manner..

corresponding ground-truth values  $\mathbf{y}_t$  for an interval  $[t_1, t_2]$ , the RMSE for this interval is formally written as  $\sqrt{\frac{1}{t_2-t_1+1} \sum_{t=t_1}^{t_2} (\mathbf{y}_t - \mathbf{y}'_t)^2}$ , the MAE is  $\frac{1}{t_2-t_1+1} \sum_{t=t_1}^{t_2} |\mathbf{y}_t - \mathbf{y}'_t|$ , and the MAPE is  $\frac{1}{t_2-t_1+1} \sum_{t=t_1}^{t_2} \frac{|\mathbf{y}_t - \mathbf{y}'_t|}{\mathbf{y}_t}$ .

#### 4.1.3 Implementation details.

All of our experiments are conducted on a server with  $2 \times$  A6000 GPU. To ensure learning stability, we set a learning rate of  $5e^{-4}$  during the three training stages, and to achieve better convergence, we use 5,000 epochs for the first stage, and 1,000 epochs for the remaining two stages.

#### 4.1.4 Baseline Method

Here, we consider an LSTM-based method for forecasting (Figure 2). This is a pure machine learning method, in contrast with our main approach, which couples a neural network with an epidemic model. We employ a model similar to the LSTM model developed in [3] which has been deployed within an ensemble framework and tested extensively in the context of COVID-19 and influenza forecasting. The model is simple and consists of one LSTM layer with hidden size 32, one dense layer with hidden size 16, a rectified linear unit activation function, and one dropout layer (dropout rate of 0.2). The output layer is a dense layer with linear activation and  $L_2$  kernel regularization with a 0.01 penalty factor. The input dataset was first segmented into several continuous five-timestamp-chunks, where the first four timestamps are used as features and the last timestamp is used as the prediction target.

We also implement a similar two-encoder-structure for the LSTM, as shown in Figure 2, to handle the two heterogeneous input datasets. The first encoder processes the zip-level privatized transaction dataset. The second encoder processes public city-level datasets. The embeddings from both encoders are concatenated and passed to the decoder, which produces the forecasts.

## 4.2 Forecasting Performance

### 4.2.1 Problem Setup.

We consider a forecasting task, where "cases" is chosen as the target feature. In other words, this means that we aim to train a forecasting model that can predict daily new infected case numbers. For all of the experiments, we split the dataset into training period  $[1, T]$  and testing period  $[T + 1, T + H]$ , where  $H$  is the forecast horizon (taken to be 28 days). The training period is used for training the parameter models and the testing period is used to evaluate the performance of our method.

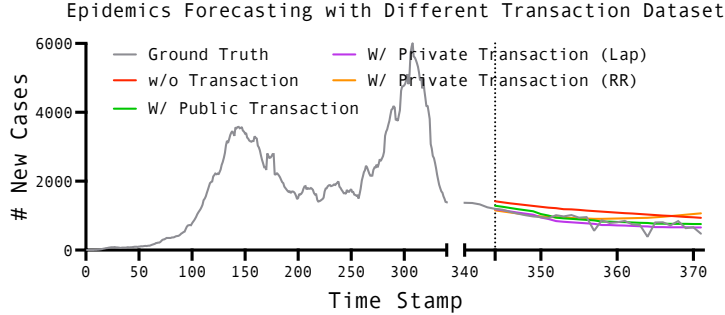


Figure 3: Forecasting using Our method with different versions of transaction dataset.

# Weeks	Metrics ↓	Baseline Method	Public Setting		Private Setting	
		LSTM	w/o Transaction	w/ Transaction	RR	Laplacian
50	RMSE	240.45	291.45	156.16	159.36	265.52
	MAE	184.49	246.96	119.85	120.35	195.63
	MAPE	28.80	29.32	19.63	18.46	24.12
54	RMSE	2732.32	2310.35	1780.13	2269.11	1832.98
	MAE	2225.35	1848.83	1410.58	1795.52	1449.52
	MAPE	76.84	59.50	45.65	57.06	46.61
58	RMSE	2143.81	2376.17	1435.11	1548.50	1270.31
	MAE	1879.32	2181.97	1180.01	1315.15	1006.56
	MAPE	35.35	49.51	30.04	27.87	24.33

Table 3: Comparison of the performance in the online setting where the length of the training data varies.

#### 4.2.2 Main Results.

We evaluate our method under four different scenarios: (1) without a transaction dataset, (2) with a public transaction dataset, (3) with a transaction dataset privatized using the Laplacian mechanism, and (4) with a transaction dataset privatized using the randomized response mechanism. Table 1 presents the main results, where we observe that incorporating the transaction dataset provides additional benefits to our epidemic model, leading to significantly lower error values. This further supports our intuition that financial data can enhance epidemic forecasting. Additionally, our method achieves lower error values compared to the baseline LSTM method, as seen in the comparison between the third and fourth columns. Beyond these advantages, we also note that the strong explainability of the meta-population model can provide valuable insights for decision-makers during a pandemic. Lastly, we find, somewhat surprisingly, that using the transaction dataset privatized with the Laplacian mechanism results in an even stronger performance than using the public dataset. Although this observation is not always consistent in the online setting (as we will demonstrate in the later section), we argue that a possible explanation for this phenomenon is that introducing noise during training enhances the model’s robustness.

### 4.3 Forecasting in the Online Setting

Table 3 presents the forecasting performance in the online setting. In other words, the training period increases by 1, 5, and 9 more weeks from the default setting (49 weeks). As shown, our method performs consistently better than the baseline LSTM method, under all the considered online forecasting experiments. We visualize the prediction of our method with the transaction dataset privatized by the Laplacian mechanism

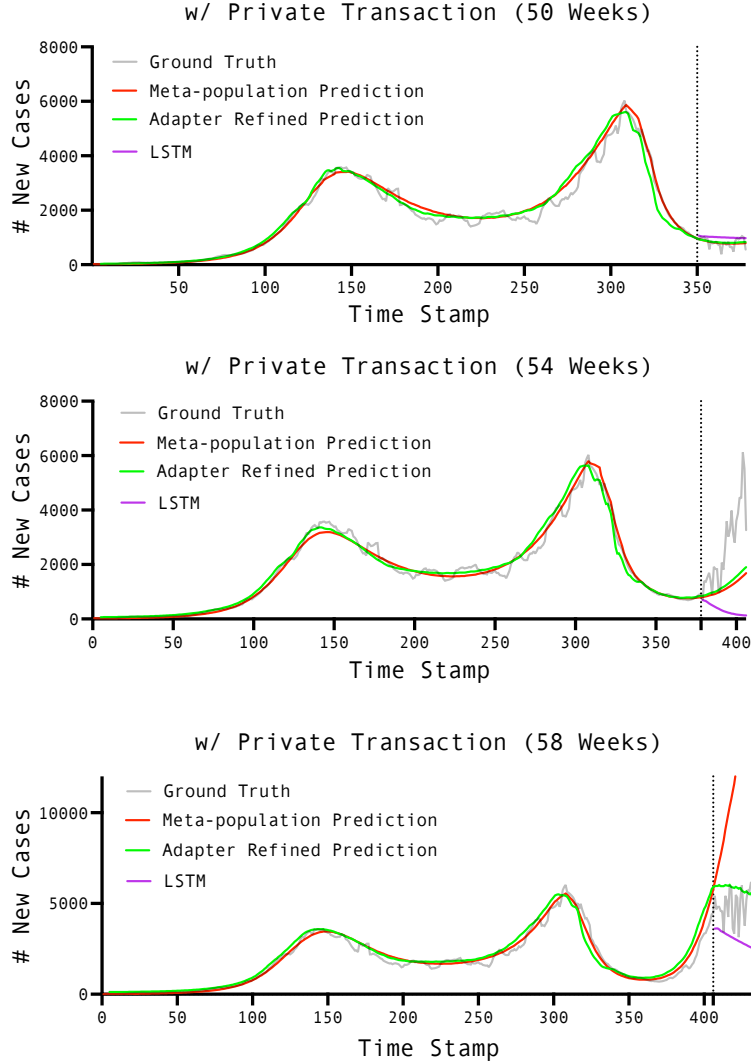


Figure 4: Visualization of the prediction in the online setting. From the top to the bottom, the training period expands from 50 weeks to 58 weeks.

( $\epsilon = 1$ ), and that of the baseline LSTM method in Figure 4. As shown, our method is better at capturing the trends of the time series. For example, for prediction in 54 weeks and 58 weeks, it is shown that the LSTM's predictions largely deviate from the trends of the case curve, while our method accurately captures the future trends. Secondly, we find that the refined prediction generated by the adapter is consistently better than that from the meta-population model, demonstrating our intuition for using the adapter as a local error correction module.

## 4.4 Analyses using privately learned epidemic model

### 4.4.1 Experimental Setups.

Suppose an intervention is introduced at some time  $T' + 7\Delta$  ( $T'$  denotes the current time (in days), so this corresponds to an intervention implemented  $\Delta$  weeks in the future), and this results in a reduction of transmission by  $x\%$ . Examples of such interventions are: (1) closures of schools or implementation of

health behaviors such as masking, in which case  $x < 0$ , and (2) large social gatherings, in which case  $x > 0$ . We assume estimates of how such interventions impact the disease model parameters are known (i.e.,  $x$  is assumed to be known). The goal is to estimate the projected number of infections after time  $T' + 7\Delta$ .

Such a question can only be studied using an epidemic model. We assume a privately learned single patch SEIRM model  $M_{inf}(\mathbf{p})$ . We use the parameters  $p(T')$  for the projection of the dynamics from time  $T' + 1$ . We change  $p(t) = (1 + x)p(T')$  for  $t \geq T' + 7\Delta$ , and estimate the number of infections in the interval  $\{T' + 1, T' + H'\}$  for a projection horizon  $H'$ . An important caveat is that there is no ground truth for such an analysis, so the model can only be evaluated based on how the model fits till time  $T'$ .

We use a simple SEIRM epidemic model with parameters  $p(T')$  learned till time  $T'$  (in days), and assume that an intervention, which changes  $\beta(t) = (1 + x)\beta(T')$ , is implemented at time  $T' + 7\Delta$ . We assume the intervention remains in position starting at  $T' + 7\Delta$ , so  $\beta(t)$  is set to

$$\beta(t) = \begin{cases} \beta(T'), & t \in \{T' + 1, T' + 7\Delta - 1\} \\ (1 - x)\beta(T'), & t \geq T' + 7\Delta \end{cases}$$

The goal is to estimate the projected number of infections after time  $T' + 7\Delta$ . We consider  $\Delta = 1$  and 2 weeks, and different values for  $x$ .

#### 4.4.2 Potential social distancing interventions.

We consider a scenario in which a social distancing type intervention is implemented, and consider  $x = -1\%$ ,  $-5\%$ ; here we discuss results using the epidemic model learned from DPEPINN. Figure 5 shows the number of infections for the learned model (in which  $\beta(t)$  keeps changing over the entire learning period), and the four interventions, in which  $\beta(t)$  is changed as described above. As expected, the number of infections increases with  $\Delta$ , and decreases with  $x$ , but the sensitivity with  $x$  is much higher.

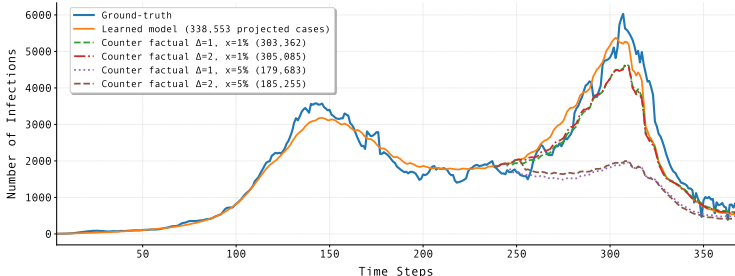


Figure 5: Analysis of interventions: the orange line shows the fit with the trained model using ground-truth data (blue line) for 52 weeks. The model trained at  $T = 231$  days is used for evaluating four interventions involving social distancing, which are implemented  $\Delta = 1, 2$  weeks after  $T$  and result in a reduction in  $\beta$  by  $x = 1\%, 5\%$ .

### 4.5 Uncertainty Quantification

Instead of providing only point predictions, we incorporate quantile predictions with confidence intervals, which are practically valuable for policymakers. To quantify uncertainty, we use multi-dimensional quantile outputs with different quantile losses, rather than the conventional MSE loss with single-dimensional outputs. Quantile loss is defined as:

$$P_\alpha = \sum_{i=t}^T \alpha\% \max(y_i - \hat{y}_i, 0) + (1 - \alpha\%) \max(\hat{y}_i - y_i, 0),$$

$\alpha = 20, 50, 80$

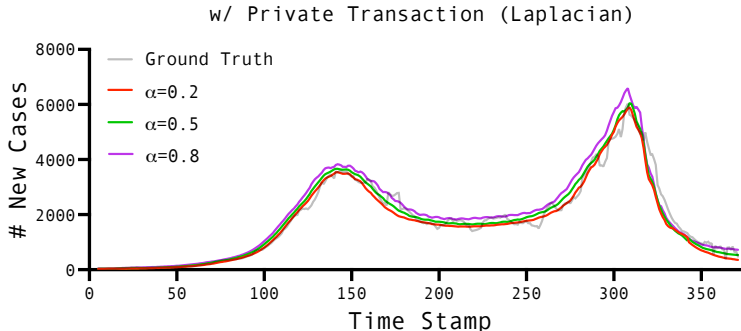


Figure 6: Performance of learning with quantile loss. We use three quantiles  $\alpha = 20, 50, 80$ .

Metrics	LSTM (Baseline)	$\epsilon = \infty$ (public)	$\epsilon = 1$	$\epsilon = 5$	$\epsilon = 10$
RMSE	302.14	285.69	233.94	220.98	250.57
MAE	251.86	302.25	289.66	203.00	223.46
MAPE	37.79	33.51	30.68	25.38	31.33

Table 4: Impact of  $\epsilon$  on the performance using the Laplacian mechanism.

Here  $y_i$  is the ground truth of the target sequence at future  $i$ -th step, and  $\hat{y}_i$  is the corresponding model estimation. Intuitively,  $P_{90}$  gives higher penalties on under-estimation, while  $P_{10}$  gives higher penalties on over-estimation. Specifically,  $\alpha = 50$  represents the median predictions;  $\alpha = 20$  gives the 20% quantile, which gives the lower bound of the confidence interval; and  $\alpha = 80$  gives the 80% quantile, which gives the upper bound of the confidence interval. In Figure 6, we show quantile predictions with confidence intervals.

## 4.6 Ablation Studies

### 4.6.1 The Impact of Mobility Dataset

Recall that the mobility dataset from Google is one of our data sources. To evaluate the impact of the mobility dataset, we compare the performance with and without the mobility dataset in the public and private settings, respectively. We observe that both the mobility datasets help in the forecast performance: the RMSE is 233.94 when both Mobility and private Transaction ( $\epsilon = 1$ ) datasets are used, which increases to 315.12 when the Mobility data is dropped. Similarly, the RMSE increases from 285.69 to 298.42 in the public setting when the mobility dataset is dropped.

### 4.6.2 The Impact of Privacy Budget $\epsilon$ .

Table 4 reports the performance of our method under different privacy budget  $\epsilon$ . As shown, our method stably achieves lower error values under different privacy budgets  $\epsilon \in \{1, 5, 10\}$ , compared to the LSTM baselines.

## 5 Related work

Even before the pandemic, the value of non-traditional data sources (compared to standard line lists and other epidemiological data) for epidemic forecasting and projection was well recognized; such datasets include different kinds of social media, e.g. [13, 2, 11, 24, 25], online search and website logs, e.g., [19, 31, 40],

Metrics	Public Setting		Private Setting ( $\epsilon = 1$ )	
	w/ Mobility	w/o Mobility	w/ Mobility	w/o Mobility
RMSE	285.69	298.42	233.94	315.12
MAE	302.25	326.67	289.66	324.52
MAPE	33.51	36.51	30.68	36.25

Table 5: Impact of mobility dataset to the performance of our method.

symptomatic online surveys, e.g., [44, 42], medical and wellness devices, e.g., [33, 26], retail and commerce data [38, 32], detailed mobility traces [39, 23], detailed disease surveillance, behavioral surveys, and financial data [35, 9, 6, 43, 4]; see survey [41]. While financial datasets have been used in public health, e.g., [35, 9, 6, 43, 4], these have been primarily focused on qualitative trends or understanding changes in specific behaviors, e.g., the level of movements and potential contacts, and less on learning epidemic models.

One area of public health where privacy was considered systematically was in the contact tracing apps developed during the pandemic, e.g., [10, 45]. There has been very limited work on public health analyses with differential privacy [28, 27]; however, the broader area of problems like forecasting and learning epidemic models with DP remains open.

## 6 Conclusions and Discussion

We present a powerful framework, DPEPiNN, for simultaneously predicting epidemic metrics and learning an epidemic model, while integrating diverse and heterogeneous datasets, including a realistic but synthetic financial transaction dataset released by data.org [1], which is used here with differential privacy guarantees. We show results using DPEPiNN for two Colombian cities, and find that adding the transaction dataset leads to better performance; for one of the cities, this holds even with DP. The privately learned epidemic model can be used for any public health task; while we showed the use of a metapopulation model within DPEPiNN, the approach can be extended to most other epidemic models, including agent-based models. Improving privacy techniques and extending the framework to other privacy models are interesting next steps.

## References

- [1] Privacy Enhancing Technologies (PETs) for public health challenge, 2024. <https://data.org/initiatives/pets-challenge/>.
- [2] Mohamed Abouzahra and Joseph Tan. Twitter vs. zika—the role of social media in epidemic outbreaks surveillance. *Health Policy and Technology*, 10(1):174–181, 2021.
- [3] Aniruddha Adiga, Lijing Wang, Benjamin Hurt, Akhil Peddireddy, Przemyslaw Porebski, Srinivasan Venkatramanan, Bryan Leroy Lewis, and Madhav Marathe. All models are useful: Bayesian ensembling for robust high resolution covid-19 forecasting. In *Proceedings of the 27th ACM SIGKDD Conference on Knowledge Discovery & Data Mining*, pages 2505–2513, 2021.
- [4] Diane Alexander and Ezra Karger. Do stay-at-home orders cause people to stay at home? effects of stay-at-home orders on consumer behavior. *Review of Economics and Statistics*, 105(4):1017–1027, 2023.

- [5] Vivek Anand, Jiaming Cui, Jack Heavey, Anil Vullikanti, and B Aditya Prakash. H2abm: Heterogeneous agent-based model on hypergraphs to capture group interactions. In *Proceedings of the 2024 SIAM International Conference on Data Mining (SDM)*, pages 280–288. SIAM, 2024.
- [6] Asger Lau Andersen, Emil Toft Hansen, Niels Johannesen, and Adam Sheridan. Consumer responses to the covid-19 crisis: Evidence from bank account transaction data. *The Scandinavian Journal of Economics*, 124(4):905–929, 2022.
- [7] Avrim Blum, Cynthia Dwork, Frank McSherry, and Kobbi Nissim. Practical privacy: The sulq framework. PODS '05, page 128–138, New York, NY, USA, 2005. Association for Computing Machinery.
- [8] Lige Cao, Xinrong Wu, Guijun Han, Wei Li, Xiaobo Wu, Haowen Wu, Chaoliang Li, Yundong Li, and Gongfu Zhou. Eakf-based parameter optimization using a hybrid adaptive method. *Monthly Weather Review*, 150(11):3065–3080, 2022.
- [9] Vasco M Carvalho, Juan R Garcia, Stephen Hansen, Álvaro Ortiz, Tomasa Rodrigo, José V Rodríguez Mora, and Pep Ruiz. Tracking the covid-19 crisis with high-resolution transaction data. *Royal Society Open Science*, 8(8):210218, 2021.
- [10] Eugene Chan and Najam Saqib. Privacy concerns can explain unwillingness to download and use contact tracing apps when covid-19 concerns are high. *Computers in Human Behavior*, 119:106718, 01 2021.
- [11] Liangzhe Chen, KSM Tozammel Hossain, Patrick Butler, Naren Ramakrishnan, and B Aditya Prakash. Flu gone viral: Syndromic surveillance of flu on twitter using temporal topic models. In *2014 IEEE international conference on data mining*, pages 755–760. IEEE, 2014.
- [12] Ayush Chopra, Alexander Rodríguez, Jayakumar Subramanian, Balaji Krishnamurthy, B Aditya Prakash, and Ramesh Raskar. Differentiable agent-based epidemiology. In *AAMAS*, 2023.
- [13] Aron Culotta. Towards detecting influenza epidemics by analyzing twitter messages. In *Proceedings of the first workshop on social media analytics*, pages 115–122, 2010.
- [14] Rachel Cummings and Deven Desai. The role of differential privacy in gdpr compliance. In *FAT'18: Proceedings of the Conference on Fairness, Accountability, and Transparency*, volume 20, 2018.
- [15] Cynthia Dwork. Differential privacy. *Encyclopedia of Cryptography and Security*, pages 338–340, 2011.
- [16] Cynthia Dwork and Aaron Roth. The algorithmic foundations of differential privacy. *Foundations and Trends in Theoretical Computer Science*, 9(3-4):211–407, 2014.
- [17] Badih Ghazi, Noah Golowich, Ravi Kumar, Pasin Manurangsi, and Chiyuan Zhang. Deep learning with label differential privacy. *Advances in neural information processing systems*, 34:27131–27145, 2021.
- [18] Badih Ghazi, Yangsibo Huang, Pritish Kamath, Ravi Kumar, Pasin Manurangsi, and Chiyuan Zhang. Labeldp-pro: Learning with label differential privacy via projections. In *The Twelfth International Conference on Learning Representations*.
- [19] Jeremy Ginsberg, Matthew H Mohebbi, Rajan S Patel, Lynnette Brammer, Mark S Smolinski, and Larry Brilliant. Detecting influenza epidemics using search engine query data. *Nature*, 457(7232):1012–1014, 2009.
- [20] Nele Goeyvaerts, Niel Hens, Benson Ogunjimi, Marc Aerts, Ziv Shkedy, Pierre Van Damme, and Philippe Beutels. Estimating infectious disease parameters from data on social contacts and serological status. *Journal of the Royal Statistical Society Series C: Applied Statistics*, 59(2):255–277, 2010.
- [21] G Harrison, J Chen, H Mortveit, S Hoops, P Porebski, D Xie, M Wilson, P Bhattacharya, A Vullikanti, L Xiong, and M Marathe. Synthetic data to support us-uk prize challenge for developing privacy enhancing methods: Predicting individual infection risk during a pandemic, 2023.

- [22] Cliff C Kerr, Robyn M Stuart, Dina Mistry, Romesh G Abeysuriya, Katherine Rosenfeld, Gregory R Hart, Rafael C Núñez, Jamie A Cohen, Prashanth Selvaraj, Brittany Hagedorn, et al. Covasim: An Agent-Based Model of COVID-19 Dynamics and Interventions. *PLOS Computational Biology*, 17(7):e1009149, 2021.
- [23] Katherine Klise, Walt Beyeler, Patrick Finley, and Monear Makvandi. Analysis of mobility data to build contact networks for covid-19. *PLoS One*, 16(4):e0249726, 2021.
- [24] Alex Lamb, Michael Paul, and Mark Dredze. Separating fact from fear: Tracking flu infections on twitter. In *Proceedings of the 2013 Conference of the North American Chapter of the Association for Computational Linguistics: Human Language Technologies*, pages 789–795, 2013.
- [25] Vasileios Lampos, Tijn De Bie, and Nello Cristianini. Flu detector-tracking epidemics on twitter. In *Machine Learning and Knowledge Discovery in Databases: European Conference, ECML PKDD 2010, Barcelona, Spain, September 20-24, 2010, Proceedings, Part III 21*, pages 599–602. Springer, 2010.
- [26] Sequoia I Leuba, Reza Yaesoubi, Marina Antillon, Ted Cohen, and Christoph Zimmer. Tracking and predicting us influenza activity with a real-time surveillance network. *PLoS computational biology*, 16(11):e1008180, 2020.
- [27] George Z Li, Dung Nguyen, and Anil Vullikanti. Differentially private partial set cover with applications to facility location. *IJCAI*, 2022.
- [28] George Z Li, Dung Nguyen, and Anil Vullikanti. Computing epidemic metrics with edge differential privacy. In *International Conference on Artificial Intelligence and Statistics*, pages 4303–4311. PMLR, 2024.
- [29] Madhav Marathe and Anil Vullikanti. Computational epidemiology. *Communications of the ACM*, 56(7):88–96, 2013.
- [30] Sarabeth M Mathis, Alexander E Webber, Tomás M León, Erin L Murray, Monica Sun, Lauren A White, Logan C Brooks, Alden Green, Addison J Hu, Roni Rosenfeld, et al. Evaluation of flusight influenza forecasting in the 2021–22 and 2022–23 seasons with a new target laboratory-confirmed influenza hospitalizations. *Nature communications*, 15(1):6289, 2024.
- [31] David J McIver and John S Brownstein. Wikipedia usage estimates prevalence of influenza-like illness in the united states in near real-time. *PLoS computational biology*, 10(4):e1003581, 2014.
- [32] Ioanna Miliou, Xinyue Xiong, Salvatore Rinzivillo, Qian Zhang, Giulio Rossetti, Fosca Giannotti, Dino Pedreschi, and Alessandro Vespignani. Predicting seasonal influenza using supermarket retail records. *PLOS Computational Biology*, 17(7):e1009087, 2021.
- [33] Aaron C Miller, Inder Singh, Erin Koehler, and Philip M Polgreen. A smartphone-driven thermometer application for real-time population-and individual-level influenza surveillance. *Clinical Infectious Diseases*, 67(3):388–397, 2018.
- [34] Dina Mistry, Maria Litvinova, Ana Pastore y Piontti, Matteo Chinazzi, Laura Fumanelli, Marcelo FC Gomes, Syed A Haque, Quan-Hui Liu, Kunpeng Mu, Xinyue Xiong, et al. Inferring high-resolution human mixing patterns for disease modeling. *Nature communications*, 12(1):323, 2021.
- [35] Nidhi Mulay, Vikas Bishnoi, Himanshi Charotia, Siddhartha Asthana, Gaurav Dhama, and Ankur Arora. Pandemic spread prediction and healthcare preparedness through financial and mobility data. In *2020 19th IEEE International Conference on Machine Learning and Applications (ICMLA)*, pages 1340–1347. IEEE, 2020.

- [36] Kobbi Nissim, Sofya Raskhodnikova, and Adam Smith. Smooth sensitivity and sampling in private data analysis. In *Proceedings of the Thirty-Ninth Annual ACM Symposium on Theory of Computing*, STOC '07, page 75–84, New York, NY, USA, 2007. Association for Computing Machinery.
- [37] NSF-NIST. Pets prize challenge: Phase 1. data track b: Pandemic forecasting transforming pandemic response and forecasting, 2023.
- [38] Elaine O Nsoesie, David L Buckeridge, and John S Brownstein. Guess who’s not coming to dinner? evaluating online restaurant reservations for disease surveillance. *Journal of medical Internet research*, 16(1):e2998, 2014.
- [39] Emanuele Pepe, Paolo Bajardi, Laetitia Gauvin, Filippo Privitera, Brennan Lake, Ciro Cattuto, and Michele Tizzoni. Covid-19 outbreak response, a dataset to assess mobility changes in italy following national lockdown. *Scientific data*, 7(1):230, 2020.
- [40] Philip M Polgreen, Forrest D Nelson, George R Neumann, and Robert A Weinstein. Use of prediction markets to forecast infectious disease activity. *Clinical Infectious Diseases*, 44(2):272–279, 2007.
- [41] Alexander Rodríguez, Harshavardhan Kamarthi, Pulak Agarwal, Javen Ho, Mira Patel, Suchet Sapre, and B. Aditya Prakash. Machine learning for data-centric epidemic forecasting. *Nature Machine Intelligence*, 2024.
- [42] Joshua A Salomon, Alex Reinhart, Alyssa Bilinski, Eu Jing Chua, Wichada La Motte-Kerr, Minttu M Rönk, Marissa B Reitsma, Katherine A Morris, Sarah LaRocca, Tamer H Farag, et al. The us covid-19 trends and impact survey: Continuous real-time measurement of covid-19 symptoms, risks, protective behaviors, testing, and vaccination. *Proceedings of the National Academy of Sciences*, 118(51):e2111454118, 2021.
- [43] Adam Sheridan, Asger Lau Andersen, Emil Toft Hansen, and Niels Johannesen. Social distancing laws cause only small losses of economic activity during the covid-19 pandemic in scandinavia. *Proceedings of the National Academy of Sciences*, 117(34):20468–20473, 2020.
- [44] Mark S Smolinski, Adam W Crawley, Kristin Baltrusaitis, Rumi Chunara, Jennifer M Olsen, Oktawia Wójcik, Mauricio Santillana, Andre Nguyen, and John S Brownstein. Flu near you: crowdsourced symptom reporting spanning 2 influenza seasons. *American journal of public health*, 105(10):2124–2130, 2015.
- [45] Cong Duc Tran and Tin Trung Nguyen. Health vs. privacy? the risk-risk tradeoff in using covid-19 contact-tracing apps. *Technology in Society*, 67:101755, 2021.
- [46] US President, Biden, Joseph R. Executive order on the safe, secure, and trustworthy development and use of artificial intelligence, 2023. <https://www.whitehouse.gov/briefing-room/presidential-actions/2023/10/30/executive-order-on-the-safe-secure-and-trustworthy-development-and-use-of-artificial-intelligence/>
- [47] Srinivasan Venkatramanan, Jiangzhuo Chen, Arindam Fadikar, Sandeep Gupta, Dave Higdon, Bryan Lewis, Madhav Marathe, Henning Mortveit, and Anil Vullikanti. Optimizing spatial allocation of seasonal influenza vaccine under temporal constraints. *PLoS computational biology*, 15(9):e1007111, 2019.